



OPEN

Essential genes *Ptgs2*, *Tlr4*, and *Ccr2* regulate neuro-inflammation during the acute phase of cerebral ischemic in mice

Hongxiang Jiang^{1,2,3}, Zhiqiang Sun^{1,2,3}, Xiwei Zhu², Fei Li^{1✉} & Qianxue Chen^{1✉}

Ischemic stroke (IS) is associated with changes in gene expression patterns in the ischemic penumbra and extensive neurovascular inflammation. However, the key molecules related to the inflammatory response in the acute phase of IS remain unclear. To address this knowledge gap, we conducted a study using Gene Set Enrichment Analysis (GSEA) on two gene expression profiles, GSE58720 and GSE202659, downloaded from the GEO database. We screened differentially expressed genes (DEGs) using GEO2R and analyzed 170 differentially expressed intersection genes for Kyoto Encyclopedia of Genes and Genomes (KEGG) pathway enrichment and Gene Ontology (GO) analysis. We also used Metascape, DAVID, STRING, Cytoscape, and TargetScan to identify candidate miRNAs and genes. The targeted genes and miRNA molecule were clarified using the mice middle cerebral artery occlusion-reperfusion (MCAO/R) model. Our findings revealed that 170 genes were correlated with cytokine production and inflammatory cell activation, as determined by GO and KEGG analyses. Cluster analysis identified 11 hub genes highly associated with neuroinflammation: *Ccl7*, *Tnf*, *Ccl4*, *Timp1*, *Ccl3*, *Ccr1*, *Sele*, *Ccr2*, *Tlr4*, *Ptgs2*, and *Il6*. TargetScan results suggested that *Ptgs2*, *Tlr4*, and *Ccr2* might be regulated by *miR-202-3p*. In the MCAO/R model, the level of *miR-202-3p* decreased, while the levels of *Ptgs2*, *Tlr4*, and *Ccr2* increased compared to the sham group. Knockdown of *miR-202-3p* exacerbated ischemic reperfusion injury (IRI) through neuroinflammation both in vivo and in vitro. Our study also demonstrated that mRNA and protein levels of *Ptgs2*, *Tlr4*, and *Ccr2* increased in the MCAO/R model with *miR-202-3p* knockdown. These findings suggest that differentially expressed genes, including *Ptgs2*, *Tlr4*, and *Ccr2* may play crucial roles in the neuroinflammation of IS, and their expression may be negatively regulated by *miR-202-3p*. Our study provides new insights into the regulation of neuroinflammation in IS.

Ischemic stroke (IS), which is caused by a lack of blood and oxygen supply to the brain¹, accounts for approximately 85% of stroke casualties. It is a major economic and social burden worldwide². Reperfusion therapy is the only effective treatment for salvaging the penumbra in IS³. However, most neuroprotective agents that have shown efficacy in preclinical trials have failed in clinical trials, highlighting the urgent need to seek alternative therapeutic targets for IS⁴. With a better understanding of the mechanisms of IS, it is now known that ischemic cell stress leads to a variety of pathogenic events, including excitotoxicity, inflammation, oxidative stress, and mitochondrial disturbances. These IS-related pathogenic events may amplify the ischemic core and impair post-stroke recovery and the regenerative response of the brain.

It is widely accepted that macrophage and microglia activation mechanisms are involved in the pathology of IS. Therefore, modulating inflammation and neurological recovery are considered promising strategies to improve long-term prognosis after ischemia-reperfusion injury (IRI)⁵. Furthermore, reactive microglia have a dual role in IS, which is directly correlated with the phenotypes of microglia. The phenotypic changes between M1 and

¹Department of Neurosurgery, Renmin Hospital of Wuhan University, 238 Jiefang Road, Wuchang District, Wuhan 430060, Hubei Province, China. ²Central Laboratory, Renmin Hospital of Wuhan University, Wuhan 430060, Hubei Province, China. ³These authors contributed equally: Hongxiang Jiang and Zhiqiang Sun. ✉email: wdf1981@163.com; chenqx6666@whu.edu.cn

M2 in microglia are similar to those in macrophages. Previous studies have suggested that modifying microglial polarization may be a potential treatment for IS⁶. In addition, neuroinflammatory therapies have been shown to have a broader treatment window compared to thrombolytic therapies⁷. To date, the inflammation process after IS has not been fully explained. Therefore, it is important to explore the patterns of genetic alterations in the acute phase of IS to identify more key genes associated with inflammation and gain new targets for intervention.

The complexity of the brain as an organ and the diversity of its cell types have hindered our understanding of the molecular basis of IS. Gene expression regulation plays a vital role in the complex biological phenomena observed in cells. Therefore, new high-throughput sequencing technologies can aid in investigating the molecular basis of the pathological processes in IS, such as neuronal apoptosis, ischemic damage, response to therapy, and inflammatory cell infiltration⁸. However, some deviation may occur due to different experimental models, ischemic time, and even differences in animal species⁹. Furthermore, there are many time-dependent events in the inflammatory response of IS, including astrocyte proliferation, microglial activation¹⁰, and clearance of dead tissue by macrophages¹¹. This cascade of inflammatory events has been found to evolve over time and involves the expression patterns of various molecules. Unfortunately, microRNAs (miRNAs) have been shown to function to play a vital role in the inflammatory cascade during cerebral IRI. Therefore, it is of theoretical importance to construct miRNA-mRNA networks to discover potential molecular therapeutic targets¹².

Therefore, we screened two mRNA datasets obtained from mice with early acute IS in the GEO database to identify key genes and miRNAs related to the development of inflammatory responses. Furthermore, we performed the stable mice MCAO/R model to validate the identified miRNAs and key genes. The temporal distribution of the three central genes in the present study was characterized to further elucidate the key molecular mechanisms of inflammation in IS, which is expected to provide the basis for effective IRI therapies.

Results

DEGs identification. We screened two microarray datasets in the GEO database to identify inflammation-related genes in IS. The GSE58720 dataset includes 3 SHAM samples and 3 MCAO samples, while the GSE202659 dataset includes 3 SHAM samples and 3 MCAO samples. The sequencing information of both datasets comes from mice and belongs to the GPL10787-9758 and GPL24247 platforms, respectively. Using the criteria of adjusted P-value < 0.05 and $|\log_{2}FC| > 0.585$, we identified 1127 DEGs in the GSE58720 data set, and 543 DEGs in the GSE202659 dataset. The volcano plot is depicted in Fig. 1A. We further filtered and mapped these genes using a Venn diagram (Fig. 1B) and found 168 overlapping genes that were differentially expressed in both datasets.

Gene set enrichment analysis (GSEA). We performed GSEA analysis using the two selected databases to gain a preliminary understanding of the main roles of all genes. All gene expression information was uploaded to the GSEA package in R, and the C2, C5, and C7 gene set databases were selected to analyze gene expression profiles. The significantly enriched gene sets were determined using a default cut-off q value < 0.25 and P-value < 0.05. It was found that both gene sets were significantly enriched in coagulation cascades, complement, and defense response (Fig. 2A,B), which may be related to neurovascular inflammation after IS.

KEGG and GO enrichment analysis of DEGs. After identifying the 168 overlapping genes, KEGG and GO enrichment analyses were conducted using Metascape and DAVID online sites. The results from the DAVID database were presented in a bubble plot (Fig. 3A). The biological processes associated with the 168 overlapping genes were found to be significantly enriched in the positive regulation of tumor necrosis factor production and inflammatory response. The cellular components enriched in the analysis were the extracellular region, cell surface, and extracellular space. For molecular function, changes were primarily enriched in chemokine activity and cytokine activity. KEGG analyses indicated that MCMs were associated with the IL-17 signaling pathway and the Toll-like receptor signaling pathway.

The results of the analysis with Metascape are presented in Fig. 3B. The overlapping genes were primarily enriched in the inflammatory response, macrophage activation, and positive regulation of response to external stimulus. The top 20 GO and KEGG enrichment items were classified into 4 functional groups: KEGG pathway (1 item), molecular function (1 item), biological process (17 items), and cellular component (1 item). The 168 overlapping genes were mainly enriched in response to wounding, inflammatory response, immune effector process, regulation of cell adhesion, regulation of cytokine production, response to lipopolysaccharide, angiogenesis, positive regulation of cell death, apoptotic signaling pathway, regulation of hemopoiesis, positive regulation of reactive oxygen species metabolic process, phagocytosis, acute inflammatory response, regeneration, negative regulation of response to external stimulus, response to interleukin-1, and response to extracellular stimulus. The cellular component associated with these genes was the membrane. The molecular function of these genes was integrin binding.

Then, we used the ClueGo plug-in of Cytoscape software to visualize the interaction network of biological processes enriched by the 168 genes. The top 14 enriched items are presented as a pie chart (Fig. 4A,B), with the following biological processes being highly enriched: regulation of inflammatory response, cytokine response, positive regulation of response to external stimulus, response to interferon-gamma, tumor necrosis factor production, cellular response to chemical stimulus, response to interferon-beta, protein kinase B signaling, regulation of inflammatory response, regulation of lymphocyte proliferation, osteoblast differentiation, epithelial to mesenchymal transition, positive regulation of protein-containing complex assembly, and regulation of epithelial cell differentiation. Most of these modules are associated with inflammatory processes and inflammatory cell activation.

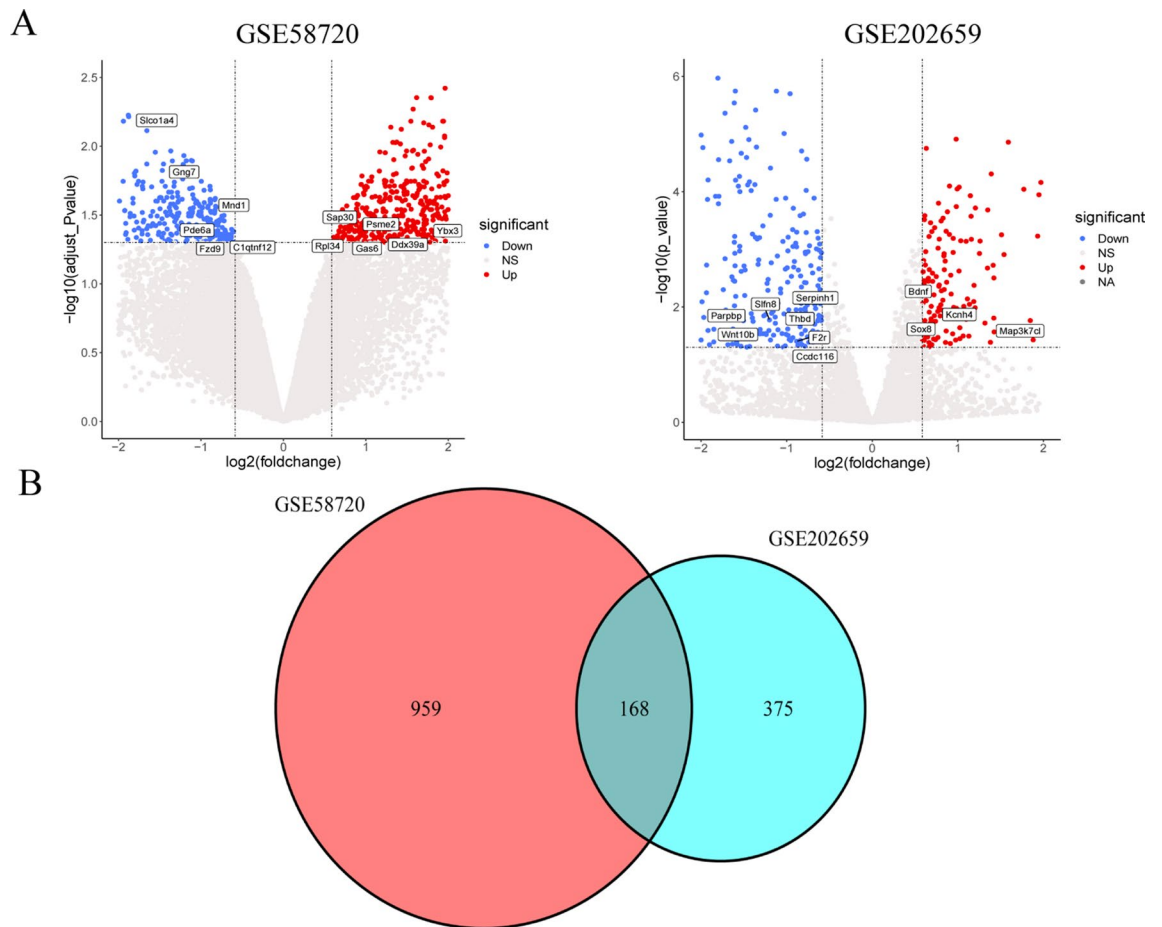


Figure 1. Identification of DEGs in the brain of rats after stroke. **(A)** Volcano plot representing DEGs between MCAO/R groups and SHAM groups shows DEGs in GSE58720 and GSE202659 datasets, respectively. **(B)** Venn diagrams showing the overlaps of numbers of DEGs between 2 selected GEO datasets.

Construction of protein–protein interaction (PPI) network for gene clusters. To identify key genes from DEGs, we uploaded the 168 intersected genes to Metascape and obtained their relationship with GO items (Fig. 5A,B). Specifically, we found that the red cluster contained genes associated with inflammatory responses. In total, 30 genes were correlated with biological processes related to inflammation. These 30 genes were *Bdkrb2*, *C1qa*, *C3ar1*, *C5ar1*, *Cebpb*, *Cxcr2*, *Ccr1*, *Ccr2*, *S1pr3*, *Fut4*, *Hck*, *Il6*, *Acod1*, *Cd180*, *Naip2*, *Ptgs2*, *S100a9*, *Ccl11*, *Ccl3*, *Ccl4*, *Ccl7*, *Sele*, *Serpina3n*, *Timp1*, *Tnf*, *Trex1*, *Tlr2*, *Ccl24*, *Pycard*, and *Ticam1*. For further analysis, we selected genes related genes to the inflammatory response.

Screening of inflammatory response related genes. To screen for genes related to the inflammatory response, we uploaded the 30 highly correlated genes to STRING and Cytoscape (Fig. 6A,B) for further analysis. The protein–protein interaction network constructed in Cytoscape showed the correlation between these 30 genes and their respective intensities, which were represented by the size and color of the bubbles. In Fig. 6B, we identified eleven hub genes that were related to the inflammatory response using the MECODE plugin in Cytoscape. These genes were *Ccl7*, *Tnf*, *Ccl4*, *Timp1*, *Ccl3*, *Ccr1*, *Sele*, *Ccr2*, *Tlr4*, *Ptgs2*, and *Il6*.

The miRNA mining and interaction network analysis. In our previous analysis, we identified 11 hub genes that were highly correlated with the inflammatory response: *Ccl7*, *Tnf*, *Ccl4*, *Timp1*, *Ccl3*, *Ccr1*, *Sele*, *Ccr2*, *Tlr4*, *Ptgs2*, and *Il6*. To further investigate the potential regulatory mechanisms of these genes, we conducted a gene–miRNA analysis using the miRWalk website. The selection criteria were based on target gene binding regions in the 3'UTR, seed match > 7 mer-1A, and context + + score percentile > 90. We used Cytoscape to construct an interaction network (Fig. 7) of the miRNAs that might regulate these genes and clarify their potential roles. Our analysis revealed that *miR-202-3p* regulates three candidate target genes, *Ptgs2*, *Tlr4*, and *Ccr2*, which may be involved in inflammatory response after IS.

Validation of key miRNAs and genes correlate with inflammation in MCAO/R model. To validate the correlation between *miR-202-3p* and *Ptgs2/Tlr4/Ccr2*, we divided mice into sham and MCAO/R groups. We obtained brain tissues from the mice MCAO/R model 24 h after ischemia–reperfusion, and confirmed the successful MCAO/R model using TTC staining (Fig. 8A). We detected the levels of miRNAs and candidate

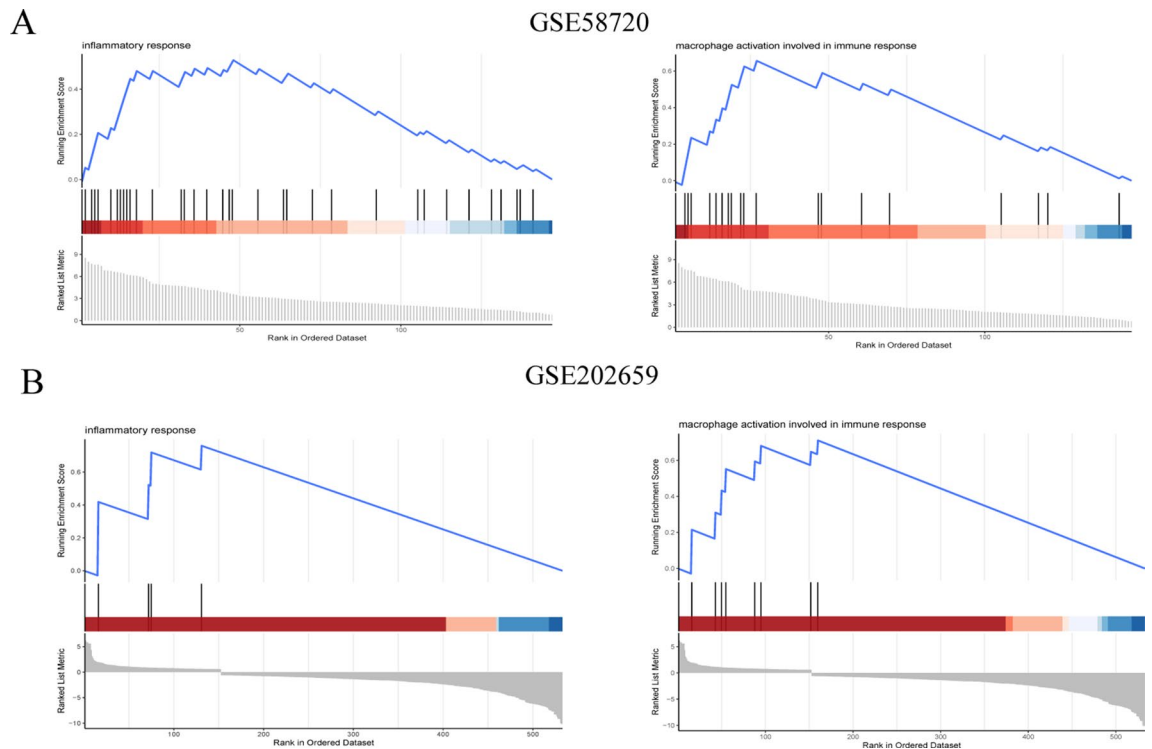


Figure 2. GSEA analysis of the two GEO datasets. **(A)** GSEA analysis results for GSE58720. **(B)** GSEA analysis results for GSE202659.

genes in the mice ischemic penumbra. The results indicated that the level of *miR-202-3p* decreased at 24 h after IRI, while the expression of *Ptgs2*, *Tlr4*, and *Ccr2* increased (Fig. 8B,C). Additionally, we conducted western blot assays to analyze the protein levels of *Ptgs2*, *Tlr4*, and *Ccr2* between the sham group and MCAO/R group, which were consistent with the results of the RT-PCR in vivo (Fig. 8D). The above results show that *miR-202-3p* could regulate three post-ischemic upregulated genes: *Ptgs2*, *Tlr4*, and *Ccr2*, which play a vital role in the acute phase of IS.

The *Ptgs2/Tlr4/Ccr2* are regulated by *miR-202-3p* in inflammation response of IS. To further provide insights into the key genes targeted in anti-inflammatory strategies, we confirmed the mechanism of three hub genes, *Ptgs2*, *Tlr4*, and *Ccr2*. Firstly, we transfected microglia cells with Anti-202-3p and related NC-Anti before the OGD/R insult. Compared to the NC-Anti group, the immuno-fluorescence results showed that the levels of iNOS increased while Arg-1 dropped in the Anti-202-3p group (Fig. 9A,B). Secondly, to further confirm the effect of *miR-202-3p* in the MCAO model, we divided mice into 4 groups: sham control group, MCAO only group, MCAO plus NC-Anti group, and MCAO plus Anti-202-3p group. The Anti-202-3p was microinjected into the lateral ventricles of the mice, and the knockdown effect of *miR-202-3p* was confirmed (Fig. 10A). After confirming that *miR-202-3p* could be stably knocked down in vivo, MCAO was performed and the neurological function scores of the mice were assessed. The findings revealed that the mice's neurological function was considerably compromised in the Anti-202-3p group and the knockdown of *miR-202-3p* could successfully rescue the brain injury after MCAO/R (Fig. 10B). Interestingly, the Anti-202-3p mice exhibited less cerebral edema (Fig. 10C), and smaller infarct volume demonstrated by TTC staining (Fig. 10D,E). Moreover, the *Ptgs2/Tlr4/Ccr2* level was upregulated when *miR-202-3p* was knocked down in the MCAO mice model (Fig. 10F–H). The protein levels for *Ptgs2/Tlr4/Ccr2* were also measured with western blot assays (Fig. 10I), indicating that the *Ptgs2/Tlr4/Ccr2* level was upregulated when *miR-202-3p* was knocked down in the MCAO mice model. We then explored the effect of *miR-202-3p* knockdown in modulating the levels of inflammatory cytokines. Two pro-inflammatory cytokines—IL-1 β and TNF- α (Fig. 10J,K) and two anti-inflammatory cytokines—IL-4 and IL-10 (Fig. 10L,M)—were measured by ELISA. After *miR-202-3p* was knocked down, the levels of TNF- α and IL-1 β increased, while the levels of IL-4 and IL-10 decreased. These promising results suggest that *miR-202-3p* regulates the *Ptgs2/Tlr4/Ccr2* genes in the inflammation response of IS.

Discussion

Persistent neuroinflammation plays an important role in many pathological processes during the acute phase of IS¹³. However, the changes in gene patterns and the specific mechanisms of inflammation have not been fully clarified¹⁴. As the treatment window continues to expand, the management of IS increasingly relies on recanalization therapy¹⁵. Unfortunately, the restoration of blood flow increases oxidative stress in ischemia tissues¹⁶ and enhances the release of pro-inflammatory cytokines¹⁷, leading to a series of pathological cascades that result in apoptosis, breakdown of the blood–brain barrier, hemorrhagic transformation, and cerebral edema. A previous

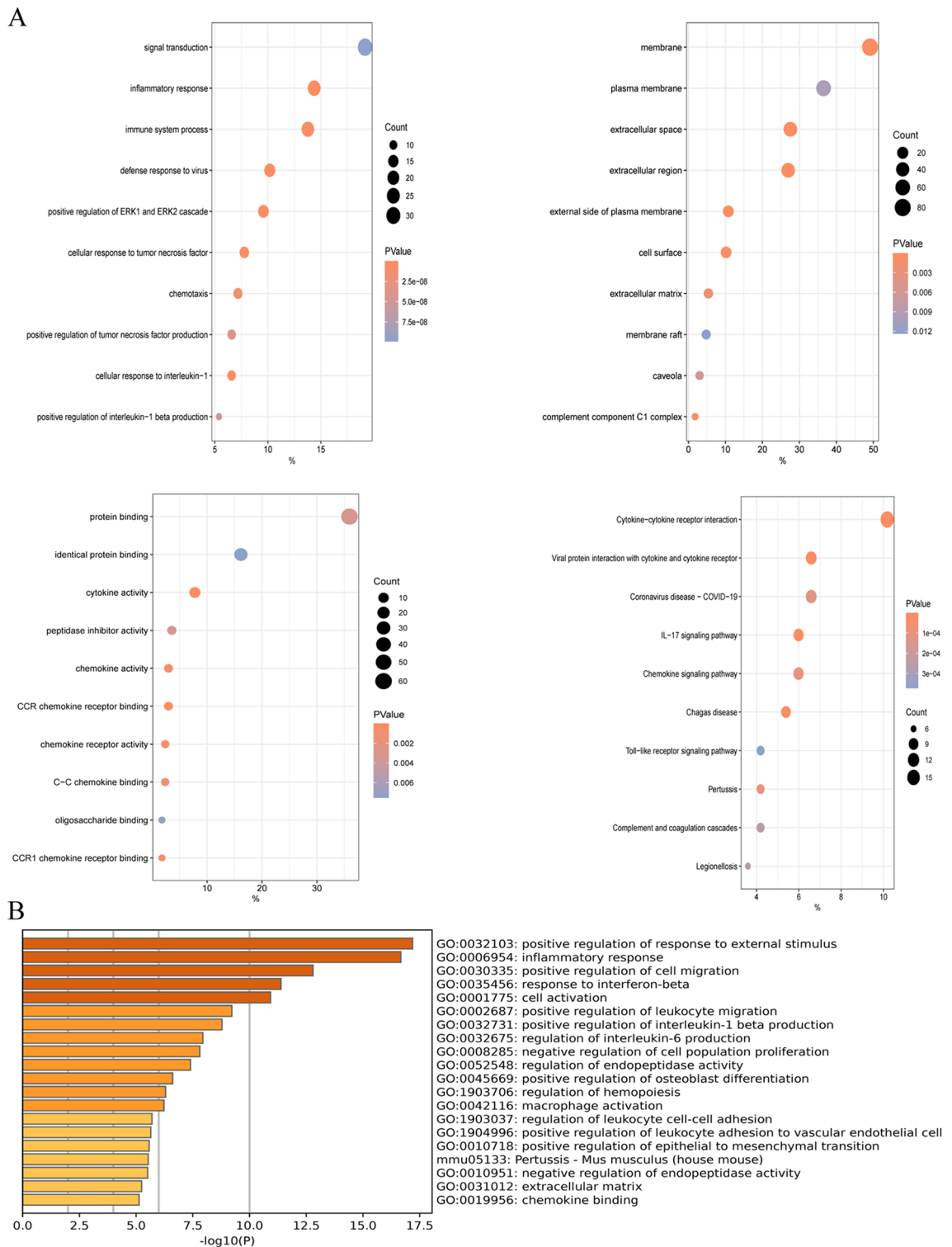
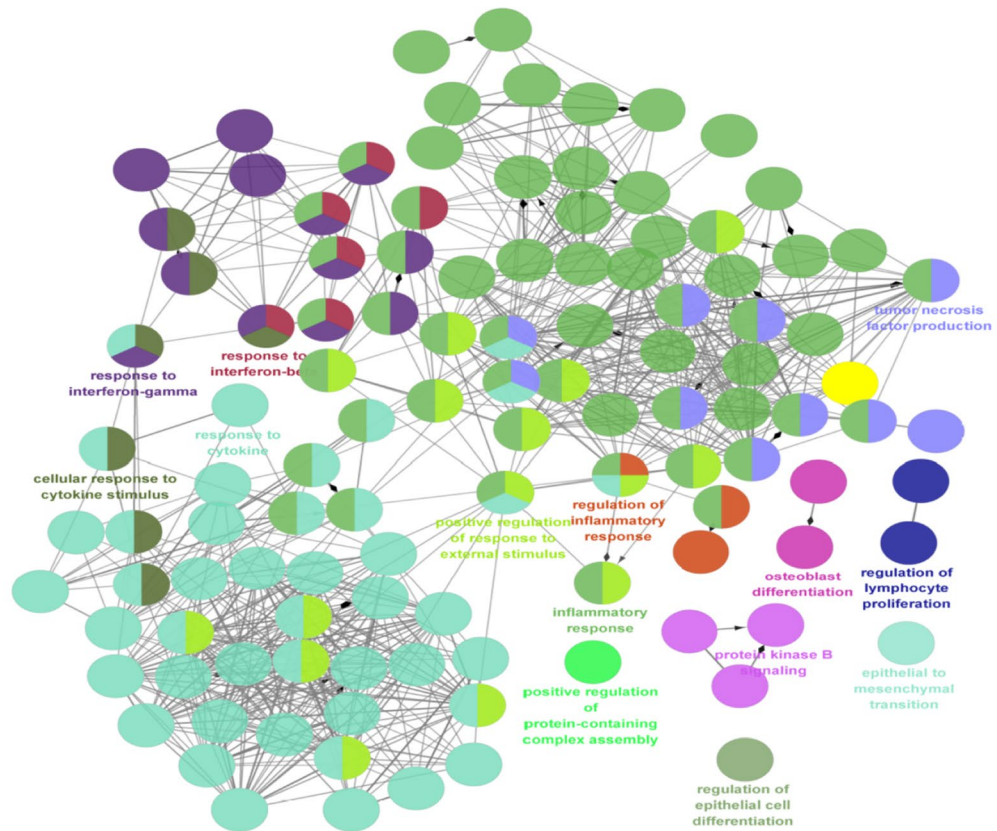


Figure 3. Functional Enrichment Analysis of DEGs. **(A)** Bubble plot of GO and KEGG enrichment analysis results from the DAVID online website⁴⁹. **(B)** Bar graph of GO and KEGG enrichment analysis results from the online website of Metascape.

study has revealed that neuroinflammatory mechanisms closely associated with oxidative stress contribute significantly to neuronal damage during the acute phase of IS¹⁸, ultimately exacerbating the extent of neurological deficit and cerebral damage caused by IRI¹⁹. However, in later stages of cerebral ischemia, neuroinflammatory pathways play an active role in tissue repair and functional recovery²⁰. In this study, we identified three genes, *Ptgs2*, *Tlr4*, and *Ccr2* by combining bioinformatics and animal experiments, and found that their expression increased during the acute phase after IRI. Theoretically, these genes are simultaneously regulated by an

A



B

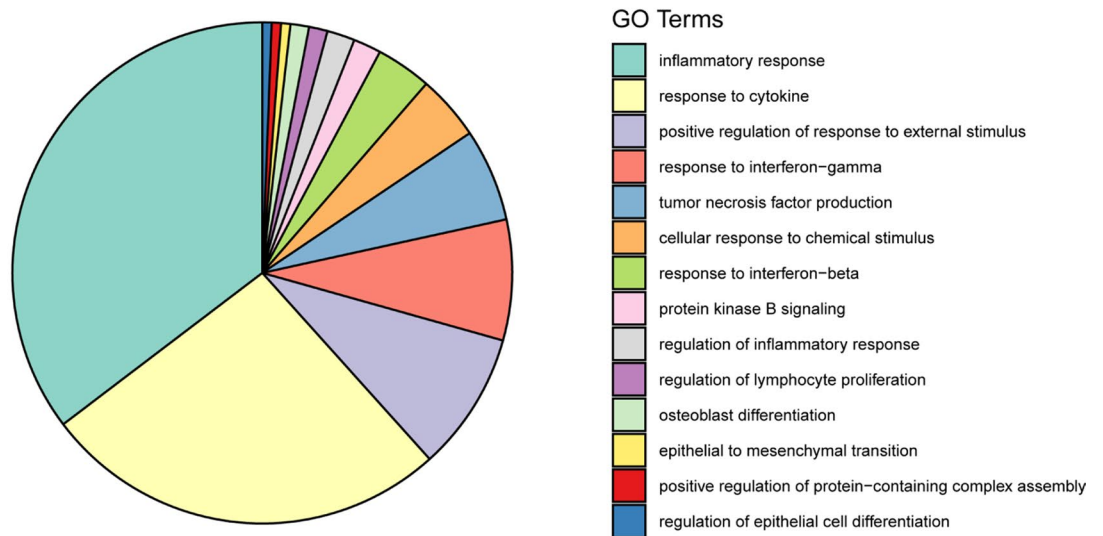


Figure 4. Functional enrichment analysis of DEGs using ClueGO. **(A)** ClueGO was used to analyze the interaction network of enriched biological processes; multiple color dots imply that a DEG is involved in multiple biological processes. **(B)** The pie charts show the enrichment of various biological processes; the gray sector represents paths with a proportion < 1.8%.

important down-regulated microRNA, *miR-202-3p*. These findings may shed light on the molecular mechanisms related to neuroinflammation in IS.

In the central nervous system (CNS), microglia are considered a major source of inflammatory mediators²¹. The sudden interruption of blood supply to the brain triggers an immune response, leading to loss of energy and neuronal damage, ultimately activating inflammatory cells²². In damaged neurons, the brain is protected from IS by various processes. Gene expression is rapidly altered, and various factors, such as ATP and glutamate, are produced, promoting the activation and migration of nearby microglia²³. Over-activated microglia are also thought to activate different inflammatory pathways, such as the nuclear factor- κ B (NF- κ B) pathway, releasing large amounts of proinflammatory mediators such as IL-1 β , IL-6, and TNF- α , leading to acute inflammatory

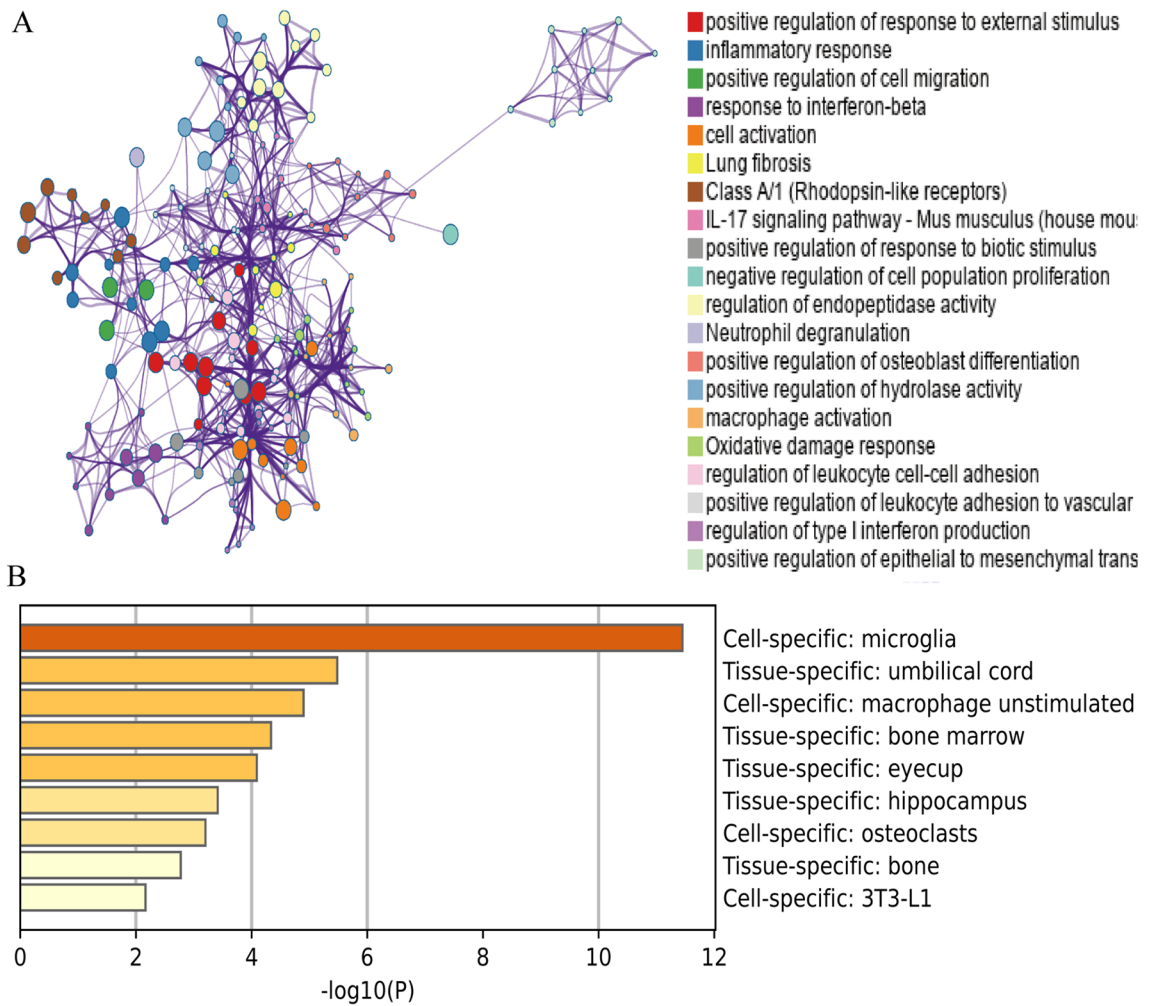


Figure 5. PPI network and function module identification. (A) Protein–protein interaction network was processed with Metascape, and different clusters were noted with different colors. (B) Major tissue and cell types associated with the DEGs.

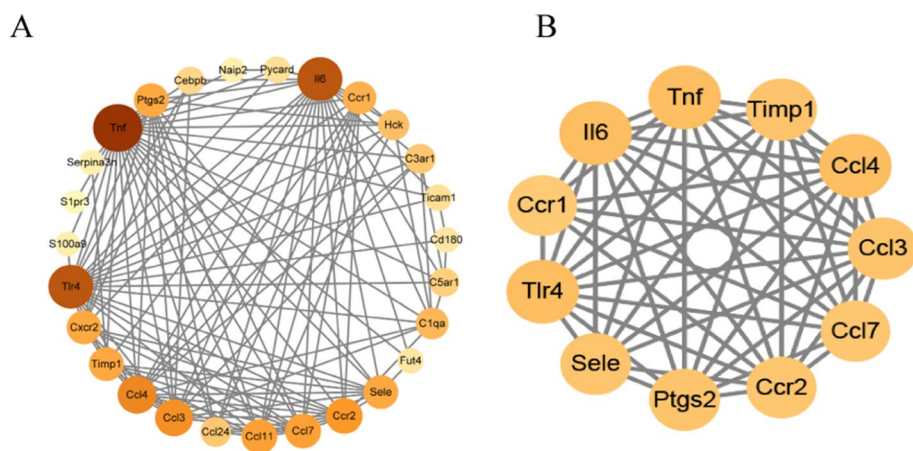


Figure 6. Multi-tools screening for genes highly associated with inflammation. (A) Cytoscape software exhibited the correlations, identified by STRING website, between the genes associated with inflammatory response; the size of circles and the depth of colors represented the correlation size. (B) The hub genes, associated with inflammatory responses, identified by MCODE function in Cytoscape software.

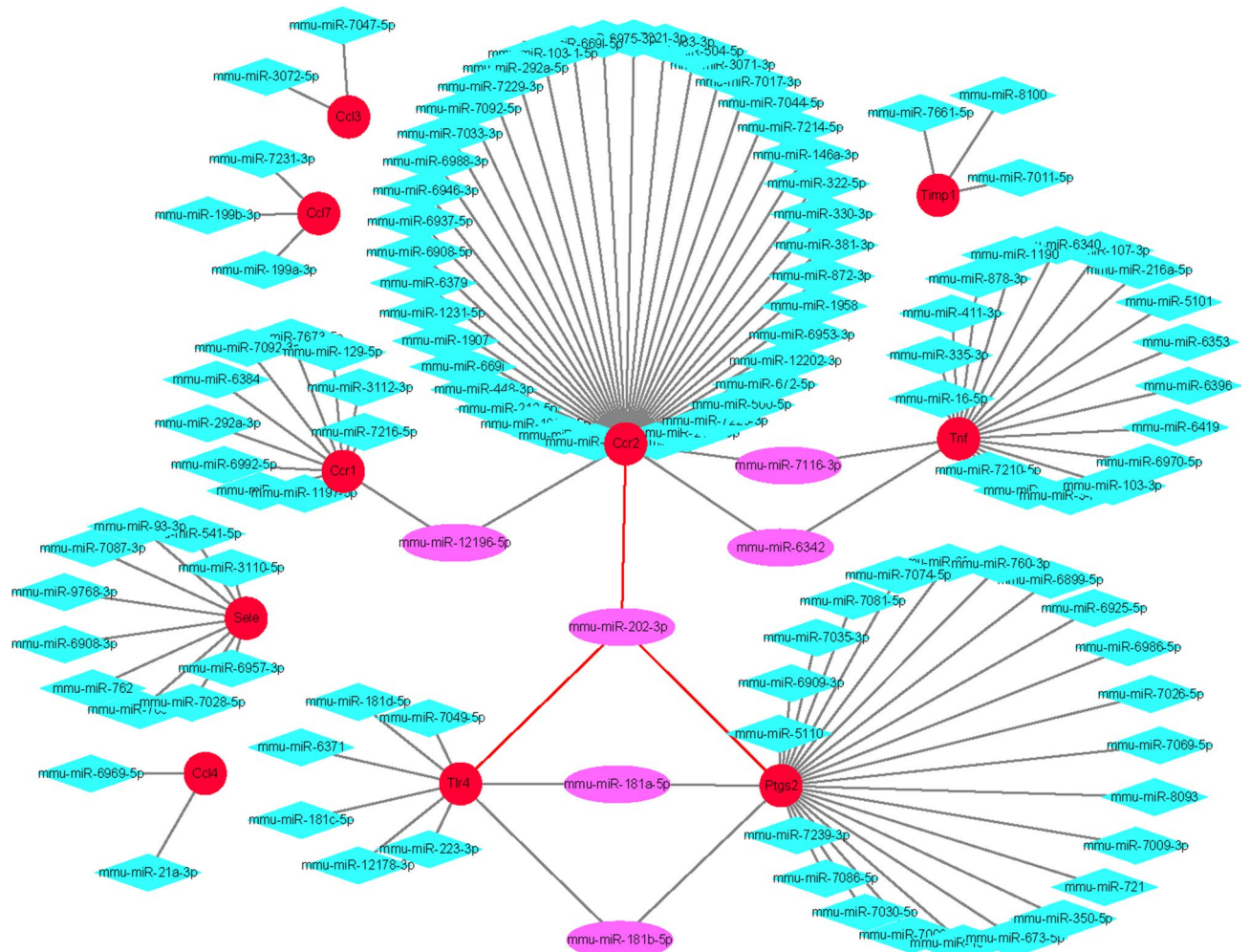


Figure 7. miRNA Prediction with Target Scan. Interaction network between genes involved in the inflammatory response and its targeted miRNAs. Genes are colored in red, and miRNAs are colored in pink, and the red lines means the connections between hub genes and hub miRNA.

reactions. Overproduction of inflammatory cytokines exacerbates neighboring neuronal damage and leads to delayed deterioration of ischemic tissue²⁴. Therefore, identifying key regulators that inhibit inflammatory factors produced by microglia and targeting these signaling molecules could prevent neuronal death after IS. Previous studies have shown that miRNAs can prevent excitotoxic injury by inhibiting post-stroke inflammation and oxidative stress in vitro and in vivo²⁵. In this study, we found that *miR-202-3p* expression was down-regulated in mice 24 h peri-infarct tissue after IRI. In contrast to previous studies, we proposed three new candidate target genes for *miR-202-3p*. This study confirms that *miR-202-3p* is a promising target for the treatment of cerebral IRI in the acute phase. Furthermore, we linked several genes to this target and explored their mutual regulation during inflammation. Our study may provide new insights into in-depth research on inflammatory mechanisms after IS.

TLR4 is a potential target gene of *miR-202-3p*. We observed significant upregulation of *TLR4* in the MCAO model. Toll-like receptors are pattern recognition receptors that recognize pathogen-associated molecular patterns and endogenous danger-associated molecular patterns²⁶. Among TLRs present in the mammalian CNS, *TLR4* is mainly expressed in microglia and mediates neuroinflammatory diseases²⁷. Previous studies have shown that the *TLR4* pathway plays a role in microglial polarization in neurodegenerative diseases such as Alzheimer's disease²⁸ and Parkinson's disease²⁹, as well as CNS trauma such as traumatic brain injury³⁰ and intracerebral hemorrhage³¹. Inhibition of *TLR4* may have a positive effect on tissue homeostasis and reduce ischemic damage in the myocardium and spinal cord³². An in vitro study has demonstrated that the activated *TLR4*/NF- κ B pathway microglial polarization to the M1 phenotype after IS³³. Our findings confirm that *TLR4* is an important factor in the regulation of the inflammatory response in the acute phase of IS and may be a potential therapeutic target.

Ptg2 is another candidate gene targeting *miR-202-3p*, a key response gene associated with homeostasis in the regulatory inflammatory response³⁴. Several studies have investigated the relationship between *Ptg2* gene polymorphisms and IS³⁵. Consistent with our study, *Ptg2* expression is significantly increased in stroke with inflammatory cell infiltration, and related studies have reported a correlation between *Ptg2* and IS³⁶. Previous studies have suggested that *Ptg2* may be associated with tumor aggressiveness and is enriched in a variety of primary endometrial tumors³⁷. During cerebral ischemia, when inflammatory cells infiltrate the injured brain,

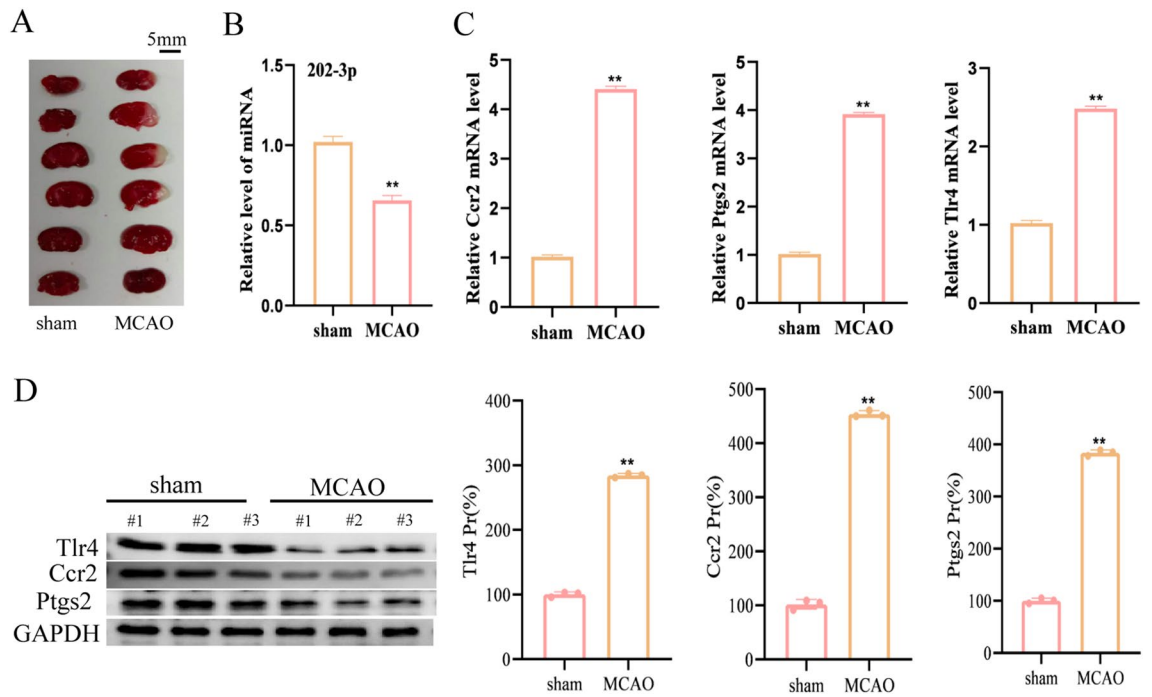


Figure 8. Validation of critical genes and miRNAs in the MCAO model. (A) TTC staining of rat MCAO model. (B) RT-PCR verification of *miR-202-3p* sham and MCAO group. (C) RT-PCR verification of critical genes between sham and MCAO group. (D) The protein levels of the targeted genes were determined in the brain tissues from the MCAO group and the sham group. Mean \pm SEM, n = 3, **p < 0.01, vs Sham group.

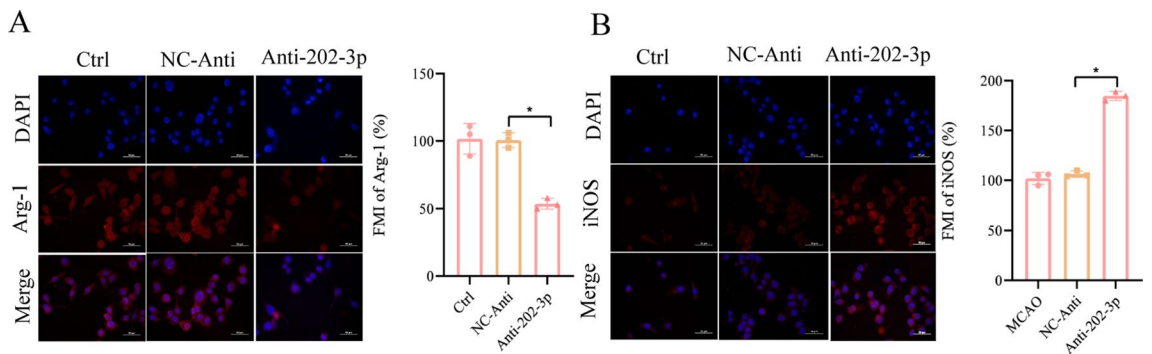


Figure 9. Knockdown of *miR-202-3p* promoted the polarization of microglia to M1 after OGD treatment. (A) Representative images of iNOS in microglia. (B) Representative images of Arg-1 in microglia. Scale bars = 50 μ m.

Ptgs2 is found to be upregulated³⁸. Furthermore, transient cerebral ischemia has been shown to induce marked apoptosis and inflammatory responses such as NF- κ B activation³⁹. Hence, *Ptgs2* is a protein closely associated with inflammatory processes and has potential applications.

In our study, we confirmed *Ccr2* as the third gene that may interact with *miR-202-3p*, which is also upregulated in the ischemic penumbra of mice. Chemokine receptor *Ccr2* is associated with the release and migration of monocytes to the ischemic brain, when activated by its ligand, *Ccl2*⁴⁰. *Ccr2/Ccl2* is known to function in many CNS disorders including ischemic encephalopathy⁴¹. However, there is no definitive conclusion regarding the role of *Ccr2*-dependent monocytes/macrophages in acute brain injury after IS. Some studies show that knockdown or pharmacological inhibition of *Ccr2* suppresses acute brain injury⁴², while others show that selective *Ccr2* antagonist causes greater damage in ischemic rat models⁴³. Hence, the exact role of *Ccr2*-dependent MoDMs remains unclear, and how they affect the recovery of brain function after IS remains largely unknown. Nevertheless, our study confirms that *Ccr2* is significantly elevated during the acute phase of IS and is modulated by *miR-202-3p*, suggesting that it may be a potential therapeutic target for IS.

Current studies on microglia phenotype have mainly focused on the process of miRNA-reducing pro-inflammatory response, with less emphasis on the anti-inflammatory effects of the M2 phenotype. Therefore, shifting the research focus to miRNAs related to the neuro-inflammatory networks would be a novel idea to study the regulation of neuroinflammation. Moreover, a more comprehensive understanding of the impact of miRNAs on

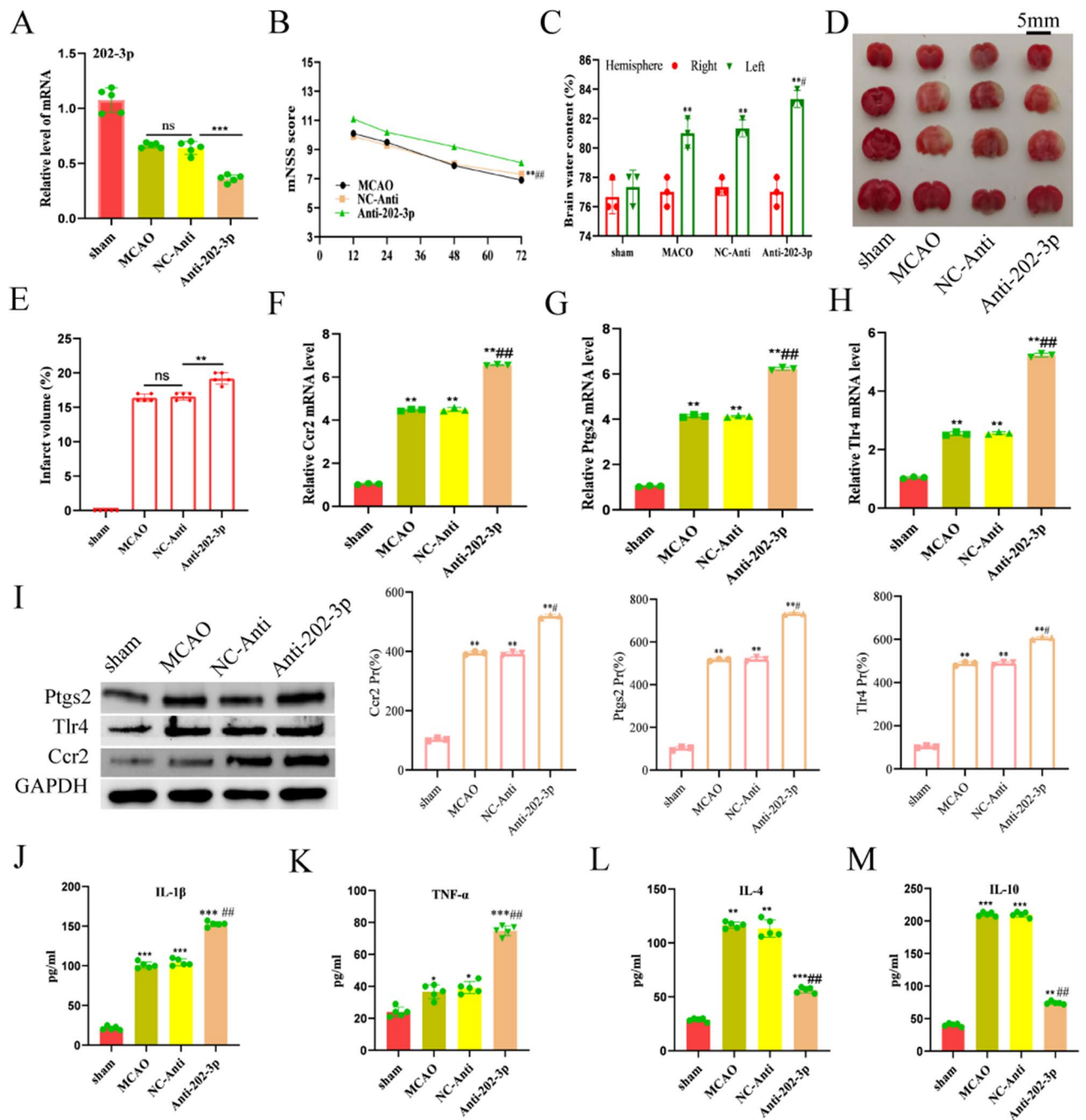


Figure 10. MiR-202-3p knockdown increased the infarct volume and pro-inflammatory cytokines after MCAO/R. **(A)** The expression of *miR-202-3p* was detected with qPCR with different treatments. Data are presented as the mean \pm SEM, $n = 5$, $***p < 0.001$ versus NC-Anti group, $ns p > 0.05$ versus MCAO/R, Mann–Whitney test. **(B)** Time-course of modified neurological severity scores. Data are presented as the mean \pm SD, $n = 5$, $**p < 0.01$ versus NC-Anti group, $##p < 0.01$ versus MCAO/R, Mann–Whitney test. **(C)** The brain water content was measured to reflect the severity of brain edema. Bars indicate the mean \pm SD, $n = 3$, $**p < 0.01$ versus sham group, $*p < 0.05$ versus sham group, $#p < 0.05$ versus NC-Anti group, t -test. **(D)** TTC-stained brain slices in sham. **(E)** Comparison of the percentages of infarct volume between each group of mice. $n = 5$, $**p < 0.01$ versus NC-Anti group, Mann–Whitney test. **(F–H)** The expression of *Ptgs2*, *Tlr4* and *Ccr2* were detected with qPCR with different treatments respectively. **(I)** The expression of *Ptgs2*, *Tlr4* and *Ccr2* were detected with the western blot with different treatments respectively. Data are presented as the mean \pm SEM, $n = 5$, $**p < 0.001$ versus NC-Anti group, $ns p > 0.05$ versus MCAO, Mann–Whitney test, $#p < 0.05$ versus NC-Anti group, t -test. An ELISA examined the protein levels of IL-1 β (**J**), TNF- α (**K**), IL-4 (**L**), and IL-10 (**M**) in the infarcted cortex at 24 h after MCAO. Data represent the mean \pm SD. $n = 5$. $*p < 0.05$, $**p < 0.01$, and $***p < 0.001$ versus sham group; $##p < 0.01$, and $###p < 0.001$ versus NC-Anti group, t -test.

neuroinflammation involving microglia may lead to the development of new therapeutic targets. For instance, utilizing miRNA delivery systems to regulate the expression of key proteins associated with specific diseases could be a promising approach⁴⁴. Current miRNA-based therapies comprise miRNA inhibitors and miRNA mimetics⁴⁵. Several immunomodulators have been shown to modulate microglial neuroinflammation by inhibiting miRNA function⁴⁶. In this study, we used bioinformatics to identify and validate the differential expression of three target genes of *miR-202-3p*, *Ptgs2*, *Tlr4*, and *Ccr2*, in the cerebral ischemia penumbra of mice. This promising new approach can help to investigate the inflammatory mechanisms of IS.

The interrelationship between the aforementioned genes and their dual role in the constantly changing inflammatory network of ischemia naturally attracted the attention of scholars. Thus, we established an interaction network between *Ptgs2*, *Tlr4*, and *Ccr2* and comprehensively analyzed their variation within the acute phase of IRI. In our study, we found that the selected three genes were significantly increased after ischemia–reperfusion, providing evidence that changes in their levels could be a potential therapeutic target. In addition, *MiR-202-3p* deduced from the gene examined in this study, was found to regulate three of the 11 key genes through bioinformatics analysis, suggesting that it plays a central role in the regulation of inflammation in the acute phase of IS. Furthermore, our study showed that *miR-202-3p* was significantly decreased and *Ptgs2*, *Tlr4*, and *Ccr2* were increased 24 h after IRI in vivo.

More attention should be given to how changes in *Ptgs2*, *Tlr4*, and *Ccr2* levels affect their function during acute IS and their interactions with *miR-202-3p*. Unfortunately, our research has some limitations. First, the inflammatory response in IS is dynamic and the results may be influenced by the timing and severity of the stroke animal model, as well as the samples collected. Second, the data analyzed were obtained from online databases and rodents. For further studies, more human tissue samples and data are required to validate our results. Additionally, the association of *miR-202-3p* with *Ptgs2*, *Tlr4*, and *Ccr2* was not directly verified, and their potential correlation mechanism in ischemic brain injury needs further investigation. Finally, using animal models to elucidate the molecular mechanisms of human disease has the drawback of difficulty in obtaining critical brain tissue from humans with IS. Therefore, studies with surgical specimens or donor brain tissue from deceased stroke patients are needed to elucidate possible mechanisms.

Conclusion

Our study suggests that the differentially expressed genes *Ptgs2*, *Tlr4*, and *Ccr2* play a critical role in regulating inflammation in IS and are negatively regulated by *miR-202-3p*. These findings provide novel insights into the complex pathophysiological mechanisms of neuroinflammation after IS.

Materials and methods

Acquisition of RNA data. The microarray expression datasets GSE58720 and GSE202659 were obtained from the GEO database (<https://www.ncbi.nlm.nih.gov/geo>). We selected 6 samples, including 3 SHAM models and 3 MCAO/R models from GSE58720. Similarly, we selected 6 samples, including 3 SHAM models and 3 MCAO/R models, from GSE202659.

Differential expression genes. The GEO2R online analysis tool (<https://www.ncbi.nlm.nih.gov/geo/geo2r/>) was used to explore the DEGs between SHAM and MCAO/R samples, and the adjusted P-value and $|\log_{10}FC|$ were calculated. Differentially expressed genes (DEGs) were defined as those with an adjusted P-value. The intersecting part was identified with the Venn diagram web tool (bioinformatics.psb.ugent.be/webtools/Venn/).

Gene set enrichment analysis (GSEA). Gene Set Enrichment Analysis (GSEA) sequenced the genes based on the differential expression levels in the two groups and then detected whether the preset gene set was enriched at the top or bottom of the sequencing table. The genetic information of the SHAM and MCAO/R samples was uploaded to R software and analyzed using the limma package.

DAVID analysis. To explore the pathways and functions of the 168 overlapping genes, we performed Gene Ontology (GO) and Kyoto Encyclopedia of Genes and Genomes (KEGG) pathways analyses with the DAVID 6.8 online tools (<https://david.ncifcrf.gov/>).

Metascape functional annotation and pathway analysis. We uploaded 170 overlapping genes to the Metascape online analysis tools (<https://metascape.org/>) to perform GO analysis, including biological process (BP), molecular function (MF), cellular component (CC), and KEGG pathway enrichment. We used the following parameters: Min Overlap = 3, P-value Cutoff = 0.01, Min Enrichment = 1.5.

Construction of protein–protein interaction (PPI) network. We inputted the DEGs into the Metascape (<https://metascape.org/>) and STRING (<https://www.string-db.org/>) online databases to obtain the protein network interaction diagram. The edges indicate both functional and physical protein associations. The line color indicates the type of interaction evidence, and the minimum required interaction score was set at medium confidence (0.4). To visualize the PPI network, we used Cytoscape software (version 3.8.2). We uploaded 168 overlapping genes to Cytoscape software to visualize the interaction network of the biological process with the Cytoscape ClueGo plug-in.

Construction of miRNA-mRNA network. The target genes from DEGs were inputted into the miR-Walk online program (<http://mirwalk.umm.uni-heidelberg.de/>) to predict the key miRNAs. Finally, the relevant results were applied to Cytoscape software to construct the mRNA-miRNA correlation network. The selection criteria were set as seed match > 7 mer-1A, the context++ score percentile > 90, and the target gene binding region was 3'UTR.

MCAO model. The MCAO surgery was performed as previously described⁴⁷. Briefly, mice were given 2% isoflurane in oxygen for 3 min, followed by 1.0–1.5% isoflurane in 70% N₂O and 30% O₂, and anesthesia was maintained by a small-animal anesthesia system. A midline neck incision was made to separate the left external carotid artery (ECA) and common carotid artery (CCA). After temporarily blocking the common and internal carotid arteries (ICA), a silicone rubber monofilament was inserted through the arteriotomy into the ECA and slowly advanced to the beginning of the middle cerebral artery (MCA) through the left ICA. After 1 h of occlusion, the monofilament was removed and the ECA was permanently ligated. For the sham group, only the monofilament was inserted into the rats to block the MCA, and then the monofilament was removed and blood flow was rapidly restored.

Quantitative real-time PCR. To extract RNA from tissues, TRIzol reagent was used. For qRT-PCR, the SYBR Green system and specific primers were utilized. The relative Ct method was used to compare the outcomes between the control and experimental groups, with β -actin serving as an internal reference. The primers used for real-time quantitative PCR (RT-qPCR) are shown in Supplementary Table 1.

Western blot analysis. Cells or tissues were washed with cold PBS and lysed with RIPA buffer containing PMSF and phosphorylated protease inhibitors. The lysates were then centrifuged at 12,000×g for 10 min at 4 °C, and the protein level in the supernatant was determined using a BCA protein assay. Next, the lysates were mixed with 5% SDS-PAGE and boiled for 10 min at 98 °C. The total proteins were loaded onto an SDS-PAGE gel and electrically transferred to a 0.22 μ M PVDF membrane. The membrane was blocked with 5% skim milk in Tris-buffered saline. The primary antibody was incubated with the membrane overnight in a ratio of 1:1000 at 4 °C. Primary antibodies are listed in Supplementary Table 2. The membrane was then incubated with Horseradish peroxidase secondary antibodies in a ratio of 1:2000 for 2 h at 25 °C. Finally, a fixed western chemiluminescent HRP substrate (Micro pores) was used to visualize the protein bands.

Oxygen–glucose deprivation (OGD). Microglia cells were obtained from the Cell Bank Type Culture Collection of the Chinese Academy of Sciences and cultured in ECM medium containing 10% fetal bovine serum (FBS), 100 μ g/ mL penicillin, and 100 μ g/ mL streptomycin at 37 °C in 5% CO₂. The cells were incubated at 37 °C with 95% N₂, and 5% CO₂ for 24 h before transfection with DMEM without glucose, after which the cells were transferred to a six-well plate. The cells were then cultured under normoxic conditions for 24 h.

Cell transfection. *MiR-202-3p* inhibitors (Anti-202-3p) and their corresponding control (NC-Anti) were purchased from Invitrogen. Microglia cells were transfected with either Anti-202-3p or NC-Anti using Lipofectamine 2000 according to the manufacturer's instructions. After transfection with NC-Anti or Anti-202-3p for 24 h, the microglia cells were exposed to either normoxia or OGD for 4 h.

Immune-fluorescence assay. The cells were fixed in 4% paraformaldehyde for 30 min, followed by permeabilization with 0.1% Triton X-100 for 10 min. Subsequently, the cells were blocked with 1% bovine serum albumin for 1 h and incubated overnight with primary antibodies specified in Supplementary Table 2. Finally, the cells were incubated with fluor-labeled secondary antibodies, and the nuclei were stained with DAPI. The images were captured using either an Olympus BX51 microscope or an Olympus FV1200 confocal microscope.

Animals. Four-week-old C57BL/6J male mice were purchased from Shulaibao Biotechnology Co., Ltd. They were housed under constant humidity and temperature and allowed free access to food and water. All mice experiments were conducted on a specific pathogen-free platform at the Experimental Animal Center of the Renmin Hospital, Wuhan University. The mice were randomly allocated into different groups and were matched for body weight. All animal experiments were approved by the Ethics Committee of Renmin Hospital of Wuhan university (Approval Number: WDRM-20200301C) and performed in line with the AAALAC and the ARRIVE guidelines.

Intracerebroventricular administration. Anti-202-3p or NC-Anti were transfected into mice brains as described previously⁴⁸. Briefly, the mice were deeply anesthetized and the plasmid premixed with transfection reagent was microinjected into the left lateral ventricle at a rate of 0.2 μ L/min. The microsyringe was left in place for 10 min after the intracerebroventricular injection. In the Sham group, mice were subjected only to a burr hole and administered an equal amount of saline through injection.

Neurobehavioral assessment. The modified neurological Severity score (mNSS) was used to assess the neurological impairment of the groups mentioned above (n = 5 in each group) at 24 h post MCAO. Neurological function was rated on a scale of 0 to 18 (normal is 0; with a maximum loss score 18 points). A score of 1 on the test indicates either the inability to perform the test or a lack of test reflexes. Therefore, a higher score indicates a more severe injury.

TTC staining. Mice were euthanized in a humanely within 24 h after MCAO. The euthanasia was performed by a rapid intravenous injection of sodium pentobarbital at 75 mg per kg of body weight. Brain tissue was excised and collected. It was immediately divided into four coronal sections. They were then incubated for 30 min with the 2% TTC solution at 37 °C before it was transferred to a 4% paraformaldehyde solution and fixed for one day. Using Image J software, we measured the extent of infarction in each section on each captured digital images.

Brain water content analysis. The brains were extracted within 24 h after MCAO and wet weights of the right and left hemispheres were calculated. To determine dry weight, the brains were boiled for 48 h at 75 °C. Subsequently, the water content of the brain was calculated as [(wet weight – dry weight)/wet weight] × 100%.

ELISA. At 24 h after MCAO, mice were anesthetized and underwent transcardial perfusion with phosphate-buffered saline (PBS, pH 7.4, 4 °C). Brain infarcts zone were immediately collected, homogenized with 200 mg/mL of 0.9% normal saline, and centrifuged at 12,000 rpm. The supernatant was collected and kept at – 80 °C. The quantities of interleukin 10 (IL-10), tumor necrosis factor alpha (TNF- α), interleukin 4 (IL-4) and interleukin 1 β (IL-1 β) in brain tissue lysates were measured using commercial ELISA kits. The ultimate concentration of cytokines was calculated from the absorbance standard curve following the manufacturer's protocol.

Statistical analysis. Statistical analysis was conducted using GraphPad Prism 8.0. All data were expressed as mean \pm SD. One-way ANOVA and t-test were performed to compare differences between groups. Each experiment was repeated three times. $P < 0.05$ was considered statistically significant.

Data availability

The raw data supporting the conclusions of this article will be made available by the authors, without undue reservation.

Received: 13 January 2023; Accepted: 7 August 2023

Published online: 10 August 2023

References

- Liu, J. *et al.* Role of phosphorylated HDAC4 in stroke-induced angiogenesis. *Biomed. Res. Int.* **2017**, 2957538 (2017).
- Kim, J. *et al.* Global stroke statistics 2019. *Int. J. Stroke* **15**(8), 819–838 (2020).
- Musuka, T. D., Wilton, S. B., Traboulsi, M. & Hill, M. D. Diagnosis and management of acute ischemic stroke: Speed is critical. *CMAJ* **187**(12), 887–893 (2015).
- Zuo, X. *et al.* MicroRNA-132 attenuates cerebral injury by protecting blood-brain-barrier in MCAO mice. *Exp. Neurol.* **316**, 12–19 (2019).
- DeLong, J. H., Ohashi, S. N., O'Connor, K. C. & Sansing, L. H. Inflammatory responses after ischemic stroke. *Semin. Immunopathol.* **44**(5), 625–648 (2022).
- Deng, L. *et al.* Long non-coding RNA ANRIL downregulation alleviates neuroinflammation in an ischemia stroke model via modulation of the miR-671-5p/NF- κ B pathway. *Neurochem. Res.* **47**(7), 2002–2015 (2022).
- Feng, Y. *et al.* miR-1224 contributes to ischemic stroke-mediated natural killer cell dysfunction by targeting Sp1 signaling. *J. Neuroinflamm.* **18**(1), 133 (2021).
- Wu, Q. *et al.* Corticotropin-releasing factor aggravates ischemic stroke injury by the inflammatory activation of microglia. *Endocrinology* **163**(3), bqac13 (2022).
- Xiao, X. *et al.* Integrated bioinformatics analysis for the identification of key molecules and pathways in the hippocampus of rats after traumatic brain injury. *Neurochem. Res.* **45**(4), 928–939 (2020).
- Pluta, R., Januszewski, S. & Czuczwar, S. J. Neuroinflammation in post-ischemic neurodegeneration of the brain: Friend, foe, or Both?. *Int. J. Mol. Sci.* **22**(9), 4405 (2021).
- Ellison, J. A., Barone, F. C. & Feuerstein, G. Z. Matrix remodeling after stroke. De novo expression of matrix proteins and integrin receptors. *Ann. N. Y. Acad. Sci.* **890**, 204–222 (1999).
- Li, G. *et al.* Impact of microRNAs on ischemic stroke: From pre- to post-disease. *Prog. Neurobiol.* **163–164**, 59–78 (2018).
- Lo, J. W. *et al.* Profile of and risk factors for poststroke cognitive impairment in diverse ethnoregional groups. *Neurology* **93**(24), e2257–e2271 (2019).
- Jin, R., Liu, L., Zhang, S., Nanda, A. & Li, G. Role of inflammation and its mediators in acute ischemic stroke. *J. Cardiovasc. Transl. Res.* **6**(5), 834–851 (2013).
- Powers, W. J. *et al.* Guidelines for the early management of patients with acute ischemic stroke: 2019 Update to the 2018 guidelines for the early management of acute ischemic stroke: A guideline for healthcare professionals from the American Heart Association/American Stroke Association [published correction appears in *Stroke*. 2019 Dec;50(12): e440–e441]. *Stroke*. **50**(12), e344–e418 (2019).
- Jurcau, A. & Ardelean, I. A. Molecular pathophysiological mechanisms of ischemia/reperfusion injuries after recanalization therapy for acute ischemic stroke. *J. Integr. Neurosci.* **20**(3), 727–744 (2021).
- Lin, L. & Wang, X. Ischemia-reperfusion injury in the brain: Mechanisms and potential therapeutic strategies. *Biochem. Pharmacol.* **5**(4), 213 (2016).
- Wong, C. H. & Crack, P. J. Modulation of neuro-inflammation and vascular response by oxidative stress following cerebral ischemia-reperfusion injury. *Curr. Med. Chem.* **15**(1), 1–14 (2008).
- Wu, L. *et al.* Targeting oxidative stress and inflammation to prevent ischemia-reperfusion injury. *Front. Mol. Neurosci.* **13**, 28 (2020).
- Chamorro, A. & Hallenbeck, J. The harms and benefits of inflammatory and immune responses in vascular disease. *Stroke* **37**(2), 291–293 (2006).
- Zhang, W. *et al.* Microglia-associated neuroinflammation is a potential therapeutic target for ischemic stroke. *Neural Regener. Res.* **16**(1), 6–11 (2021).
- Iadecola, C., Buckwalter, M. S. & Anrather, J. Immune responses to stroke: Mechanisms, modulation, and therapeutic potential. *J. Clin. Invest.* **130**(6), 2777–2788 (2020).
- Bernaus, A., Blanco, S. & Sevilla, A. Glia crosstalk in neuroinflammatory diseases. *Front. Cell Neurosci.* **14**, 209 (2020).
- Li, X. *et al.* Mib2 deficiency inhibits microglial activation and alleviates ischemia-induced brain injury. *Aging Dis.* **11**(3), 523–535 (2020).

25. Xu, L. J., Ouyang, Y. B., Xiong, X., Stary, C. M. & Giffard, R. G. Post-stroke treatment with miR-181 antagomir reduces injury and improves long-term behavioral recovery in mice after focal cerebral ischemia. *Exp. Neurol.* **264**, 1–7 (2015).
26. Anttila, J. E., Whitaker, K. W., Wires, E. S., Harvey, B. K. & Airavaara, M. Role of microglia in ischemic focal stroke and recovery: Focus on Toll-like receptors. *Prog. Neuropsychopharmacol. Biol. Psychiatry* **79**(Pt A), 3–14 (2017).
27. Zhang, L. *et al.* Vagus nerve stimulation mediates microglia M1/2 polarization via inhibition of TLR4 pathway after ischemic stroke. *Biochem. Biophys. Res. Commun.* **577**, 71–79 (2021).
28. Cui, W. *et al.* Inhibition of TLR4 induces M2 microglial polarization and provides neuroprotection via the NLRP3 inflammasome in Alzheimer's disease. *Front. Neurosci.* **14**, 444 (2020).
29. Azam, S. *et al.* Regulation of toll-like receptor (TLR) signaling pathway by polyphenols in the treatment of age-linked neurodegenerative diseases: Focus on TLR4 signaling. *Front. Immunol.* **10**, 1000 (2019).
30. Yao, X. *et al.* TLR4 signal ablation attenuated neurological deficits by regulating microglial M1/M2 phenotype after traumatic brain injury in mice. *J. Neuroimmunol.* **310**, 38–45 (2017).
31. Sun, Z. *et al.* IGF-1R stimulation alters microglial polarization via TLR4/NF- κ B pathway after cerebral hemorrhage in mice. *Brain Res. Bull.* **164**, 221–234 (2020).
32. Bell, M. T. *et al.* Toll-like receptor 4-dependent microglial activation mediates spinal cord ischemia-reperfusion injury. *Circulation* **128**(11 Suppl 1), S152–S156 (2013).
33. Ran, Y. *et al.* Baicalein ameliorates ischemic brain damage through suppressing proinflammatory microglia polarization via inhibiting the TLR4/NF- κ B and STAT1 pathway. *Brain Res.* **1770**, 147626 (2021).
34. Zhou, Z. *et al.* Silencing of PTGS2 exerts promoting effects on angiogenesis endothelial progenitor cells in mice with ischemic stroke via repression of the NF- κ B signaling pathway. *J. Cell Physiol.* **234**(12), 23448–23460 (2019).
35. Wu, G. *et al.* Influence of the cyclooxygenase-2 gene-765G/C and -1195G/A polymorphisms on development of ischemic stroke. *J. Stroke Cerebrovasc. Dis.* **25**(9), 2126–2135 (2016).
36. Zhang, Z. *et al.* Genetic variation of inflammatory genes to ischemic stroke risk in a Chinese Han population. *Pharmgenom. Pers. Med.* **14**, 977–986 (2021).
37. St-Germain, M. E., Gagnon, V., Parent, S. & Asselin, E. Regulation of COX-2 protein expression by Akt in endometrial cancer cells is mediated through NF- κ B/IkappaB pathway. *Mol. Cancer* **3**, 7 (2004).
38. Iadecola, C. *et al.* Reduced susceptibility to ischemic brain injury and N-methyl-D-aspartate-mediated neurotoxicity in cyclooxygenase-2-deficient mice. *Proc. Natl. Acad. Sci. U S A.* **98**(3), 1294–1299 (2001).
39. Wen, Y. *et al.* Estrogen attenuates nuclear factor- κ B activation induced by transient cerebral ischemia. *Brain Res.* **1008**(2), 147–154 (2004).
40. Fang, W. *et al.* CCR2-dependent monocytes/macrophages exacerbate acute brain injury but promote functional recovery after ischemic stroke in mice. *Theranostics* **8**(13), 3530–3543 (2018).
41. He, S. *et al.* Propagermanium, a CCR2 inhibitor, attenuates cerebral ischemia/reperfusion injury through inhibiting inflammatory response induced by microglia. *Neurochem. Int.* **125**, 99–110 (2019).
42. Chu, H. X. *et al.* Role of CCR2 in inflammatory conditions of the central nervous system. *J. Cereb. Blood Flow Metab.* **34**(9), 1425–1429 (2014).
43. Chu, H. X. *et al.* Evidence that Ly6C(hi) monocytes are protective in acute ischemic stroke by promoting M2 macrophage polarization. *Stroke* **46**(7), 1929–1937 (2015).
44. Zhang, L., Li, Y. J., Wu, X. Y., Hong, Z. & Wei, W. S. MicroRNA-181c negatively regulates the inflammatory response in oxygen-glucose-deprived microglia by targeting Toll-like receptor 4. *J. Neurochem.* **132**(6), 713–723 (2015).
45. Sun, P., Liu, D. Z., Jickling, G. C., Sharp, F. R. & Yin, K. J. MicroRNA-based therapeutics in central nervous system injuries. *J. Cereb. Blood Flow Metab.* **38**(7), 1125–1148 (2018).
46. Martinez, B. & Peplow, P. V. Immunomodulators and microRNAs as neurorestorative therapy for ischemic stroke. *Neural Regen. Res.* **12**(6), 865–874 (2017).
47. Engel, O., Kolodziej, S., Dirnagl, U. & Prinz, V. Modeling stroke in mice - middle cerebral artery occlusion with the filament model. *J. Vis. Exp.* **47**, 2423 (2011).
48. Xie, J. *et al.* Inhibition of NOX4/ROS suppresses neuronal and blood-brain barrier injury by attenuating oxidative stress after intracerebral hemorrhage. *Front. Cell Neurosci.* **14**, 578060 (2020).
49. Kanehisa, M., Furumichi, M., Sato, Y., Kawashima, M. & Ishiguro-Watanabe, M. KEGG for taxonomy-based analysis of pathways and genomes. *Nucleic Acids Res.* **51**(D1), D587–D592 (2023).

Acknowledgements

The authors would like to thank all the reviewers who participated in the review, as well as MJEditor (www.mjeditor.com) for providing English editing services during the preparation of this manuscript.

Author contributions

Q.C. and F.L. have contributed to study conception and design. H.J. and Z.S. and X.Z. have contributed to result interpretation and manuscript drafting. H.J. has contributed to the IHC experiments and statistical analysis. Z.S. and F.L. have contributed to interpretation of the study results and critical revision for important intellectual contents. All authors reviewed the manuscript.

Funding

This work was supported by the National Natural Science Foundation of China (No.82071299).

Competing interests

The authors declare no competing interests.

Additional information

Supplementary Information The online version contains supplementary material available at <https://doi.org/10.1038/s41598-023-40255-w>.

Correspondence and requests for materials should be addressed to F.L. or Q.C.

Reprints and permissions information is available at www.nature.com/reprints.

Publisher's note Springer Nature remains neutral with regard to jurisdictional claims in published maps and institutional affiliations.



Open Access This article is licensed under a Creative Commons Attribution 4.0 International License, which permits use, sharing, adaptation, distribution and reproduction in any medium or format, as long as you give appropriate credit to the original author(s) and the source, provide a link to the Creative Commons licence, and indicate if changes were made. The images or other third party material in this article are included in the article's Creative Commons licence, unless indicated otherwise in a credit line to the material. If material is not included in the article's Creative Commons licence and your intended use is not permitted by statutory regulation or exceeds the permitted use, you will need to obtain permission directly from the copyright holder. To view a copy of this licence, visit <http://creativecommons.org/licenses/by/4.0/>.

© The Author(s) 2023